



Enhancing the
subgrid land surface
representation in
land surface models

Y. Ke et al.

Enhancing the representation of subgrid land surface characteristics in land surface models

Y. Ke^{1,2}, L. R. Leung², M. Huang², and H. Li²

¹Base of the State Key Laboratory of Urban Environment Process and Digital Modelling, Department of Resource Environment and Tourism, Capital Normal University, 105 Xi San Huan Bei Lu, Beijing, 100048, China

²Pacific Northwest National Laboratory, 902 Battelle Boulevard, Richland, Washington, WA 99352, USA

Received: 6 February 2013 – Accepted: 12 March 2013 – Published: 28 March 2013

Correspondence to: L. R. Leung (ruby.leung@pnnl.gov)

Published by Copernicus Publications on behalf of the European Geosciences Union.

Title Page

Abstract

Introduction

Conclusions

References

Tables

Figures



Back

Close

Full Screen / Esc

Printer-friendly Version

Interactive Discussion



Abstract

Land surface heterogeneity has long been recognized as important to represent in the land surface models. In most existing land surface models, the spatial variability of surface cover is represented as subgrid composition of multiple surface cover types. In this study, we developed a new subgrid classification method (SGC) that accounts for the topographic variability of the vegetation cover. Each model grid cell was represented with a number of elevation classes and each elevation class was further described by a number of vegetation types. The numbers of elevation classes and vegetation types were variable and optimized for each model grid so that the spatial variability of both elevation and vegetation can be reasonably explained given a pre-determined total number of classes. The subgrid structure of the Community Land Model (CLM) was used as an example to illustrate the newly developed method in this study. With similar computational burden as the current subgrid vegetation representation in CLM, the new method is able to explain at least 80% of the total subgrid Plant Functional Types (PFTs) and greatly reduced the variations of elevation within each subgrid class compared to the baseline method where a single elevation class is assigned to each subgrid PFT. The new method was also evaluated against two other subgrid methods (SGC1 and SGC2) that assigned fixed numbers of elevation and vegetation classes for each model grid with different perspectives of surface cover classification. Implemented at five model resolutions (0.1°, 0.25°, 0.5°, 1.0° and 2.0°) with three maximum-allowed total number of classes N_{class} of 24, 18 and 12 representing different computational burdens over the North America (NA) continent, the new method showed variable performances compared to the SGC1 and SGC2 methods. However, the advantage of the SGC method over the other two methods clearly emerged at coarser model resolutions and with moderate computational intensity ($N_{class} = 18$) as it explained the most PFTs and elevation variability among the three subgrid methods. Spatially, the SGC method explained more elevation variability in topography-complex areas and more vegetation variability in flat areas. Furthermore, the variability of both elevation

GMDD

6, 2177–2212, 2013

Enhancing the subgrid land surface representation in land surface models

Y. Ke et al.

[Title Page](#)

[Abstract](#)

[Introduction](#)

[Conclusions](#)

[References](#)

[Tables](#)

[Figures](#)



[Back](#)

[Close](#)

[Full Screen / Esc](#)

[Printer-friendly Version](#)

[Interactive Discussion](#)



and vegetation explained by the new method was more spatially homogeneous regardless of the model resolutions and computational burdens. The SGC method will be implemented in CLM over the NA continent to assess its impacts on simulating land surface processes.

1 Introduction

As the terrestrial component of earth system models, land surface models play important roles in representing the interactions between terrestrial biosphere and atmosphere, which is important for predicting future states of the earth system and assessing anthropogenic impacts on the climate system. Using land surface parameters and meteorological forcing data as input, land surface models simulate key land processes such as photosynthesis, respiration, and evapotranspiration that regulate mass, energy, moisture, and momentum exchanges between soil, vegetation and atmosphere. Because terrestrial processes are sensitive to environmental drivers, realistic representation of land surface characteristics is important for accurate estimation of surface heat fluxes, terrestrial water storages and surface CO₂ exchange required by atmospheric models. Biases in land surface representation can lead to incorrect surface water and energy partitioning, and hence, inaccurate predictions of earth system change.

As a prominent feature of the landscape, land surface heterogeneity has long been recognized as important to represent, and has increasingly been incorporated in land surface models. It has been well established that subgrid spatial variability in land surface characteristics such as vegetation cover, soil moisture, and topography can significantly affect the estimation of surface evapotranspiration, runoff, surface albedo, snowpack, and other fluxes (Koster and Suarez, 1992; Seth et al., 1994; Ghan et al., 1997; Giorgi and Avissar, 1997; Giorgi et al., 2003; Li and Arora, 2012; Li et al., 2013). For example, Seth et al. (1994) reported that incorporation of subgrid scale inhomogeneity in land surface and climate forcing in the Biosphere-Atmosphere Transfer Scheme (BATS) model resulted in 30–60% change in runoff and energy partitioning

Enhancing the subgrid land surface representation in land surface models

Y. Ke et al.

Title Page

Abstract

Introduction

Conclusions

References

Tables

Figures



Back

Close

Full Screen / Esc

Printer-friendly Version

Interactive Discussion



Enhancing the subgrid land surface representation in land surface models

Y. Ke et al.

Title Page

Abstract

Introduction

Conclusions

References

Tables

Figures

⏪

⏩

◀

▶

Back

Close

Full Screen / Esc

Printer-friendly Version

Interactive Discussion

compared to homogeneous representation of land surface. Oleson et al. (2000) and Bonan et al. (2002a, b) found that replacing a single biome representation with plant functional types (PFTs) composition within each model grid cell caused considerable change in ground temperature, evaporation and albedo.

Among the land surface parameters, vegetation plays a key role in land-surface water and energy partitioning and carbon cycle. An accurate representation of vegetation distribution and properties is important in determining the spatial patterns of energy fluxes and biogeochemical cycling. Current land surface models widely adopt the concept of PFT to describe vegetation distributions (Oleson and Bonan, 2000; Krinner et al., 2005, Ek et al., 2003; Sitch, et al., 2003; Niu et al., 2011). For example, the Noah land surface model incorporates 13 PFTs (Ek et al., 2003), CLM has 15 PFTs (Oleson et al., 2010), and ORCHIDEE distinguishes 12 PFTs (Krinner et al., 2012). While some models such as Noah represent a single dominant PFT in each model grid, models such as CLM represents subgrid spatial heterogeneity of vegetation distribution with a composition of multiple PFTs coexisting within each model grid. This representation mainly focused on the fractional coverage of each PFT and assumes that all plants of the same type cluster as a “tile” within a model grid. The location of the PFTs, however, has seldom been explicitly described (Niu et al., 2011).

In addition to horizontal landscape variability, spatial heterogeneity in topography is also a pronounced land surface characteristic and has been considered in some land surface simulations to help parameterize topographic variability in precipitation, temperature and snow processes (Leung and Ghan, 1995; Nijssen et al., 2001; Giorgi et al., 2003). Topography also affects vegetation distribution especially on scales less than 100 km (Leung and Ghan, 1998; Vankat, 1982; Barbour et al., 1987; Brown, 1994). When combined, topography and vegetation have coupled effects on surface water and energy fluxes. However, conventional subgrid methods usually considered only one parameter, i.e. either vegetation or topography distribution. Leung and Ghan (1995, 1998) developed a subgrid parameterization to incorporate the influence of topography on precipitation and snow cover and reported improved simulations in a regional

climate model that used the subgrid parameterization with an explicit grid resolution of 90 km compared to simulations performed at a finer resolution of 30 km but without the subgrid parameterization. The method facilitated coupling with a distributed hydrologic model for hydrologic simulations at the watershed scale (Leung et al., 1996), and was also found to perform well in global simulations (Ghan et al., 2006). The subgrid parameterization of Leung and Ghan (1998) is one of few that incorporate the joint distribution of both parameters. Taking advantage of the relationship between topography and vegetation, their method classifies the topography within each model grid into subgrid elevation bands and parameterizes subgrid vegetation variability by considering vegetation distribution in each elevation band. Although only one dominant vegetation type for each elevation class was considered because of the computation limit, this approach resulted in improved surface temperature simulation.

This study generalizes the method of Leung and Ghan (1998) and aims to develop an improved and efficient subgrid scheme based on high-resolution satellite-based land cover and topography products in order to enhance the representation of both vegetation cover and topography. We chose the subgrid structure of CLM as an example and used the plant functional types defined in CLM to represent vegetation. CLM is a land model within the Community Earth System Model (CESM), formerly known as Community Climate System Model (CCSM). It was designed for coupling with atmospheric models such as Community Atmosphere Model (CAM) and has been widely applied at continental to global scales to understand the impact of land processes on climate change (Oleson et al., 2010).

The spatial heterogeneity of land surface parameters in CLM is represented using a nested subgrid hierarchy. Each grid cell is composed of a different number of land units including glacier, lake, wetland, urban and vegetated surfaces. Vegetated surfaces are represented with composition of 15 possible Plant Functional Types (PFTs) such as Temperate Needleleaf Evergreen trees, Temperate Broadleaf Evergreen trees, etc., plus bare ground. In the current version of CLM (CLM 4.0), the PFT data is available at 0.5° and 0.05° resolutions (Lawrence and Chase, 2007; Lawrence et al., 2011;

Enhancing the subgrid land surface representation in land surface models

Y. Ke et al.

Title Page

Abstract

Introduction

Conclusions

References

Tables

Figures



Back

Close

Full Screen / Esc

Printer-friendly Version

Interactive Discussion



Ke et al., 2012) and the spatial distribution of each PFT within a model grid is not explicitly represented.

In this study, we developed a new subgrid PFT scheme in which the subgrid topographic distribution of PFTs was described for each model grid. This requires classification of both vegetation types and elevation. The combined classification of subgrid topography and vegetation types can be computationally intensive in terrain-complex and species-rich area because a considerable number of elevation classes are needed to represent the diverse topographic relief while multiple vegetation types are required to explain a reasonable amount of vegetation variability. The method developed in this study assigned a flexible number of elevation bands and PFTs for each model grid and optimized to explain a maximal amount of elevation and vegetation variations in a computationally efficient manner. The method is applied to North America (NA) at different model resolutions and evaluated by comparing it with other subgrid methods that use a fixed number of subgrid elevation bands and vegetation types.

2 Method

2.1 Plant Functional Types mapping

The PFT map for North America was generated at 500 m resolution based on the MODIS land cover product and climate data following the method presented in Ke et al. (2012). Briefly, seven PFTs including Needleleaf Evergreen trees, Needleleaf Deciduous trees, Broadleaf Evergreen trees, Broadleaf Deciduous trees, shrub, grass and crop were directly determined from the MODIS MCD12Q1 C5 PFT classifications for each 500 m pixel. The WorldClim 5 arc-minute (0.0833°) (Hijmans et al., 2005) climatological global monthly surface air temperature and precipitation data was interpolated to the 500 m grids and the climate rules described by Bonan et al. (2002a) were used to reclassify the 7 PFTs into 15 PFTs in the tropical, temperate and boreal climate groups. Similar to Lawrence and Chase (2007), the fractions of C3 and C4 grasses

Enhancing the subgrid land surface representation in land surface models

Y. Ke et al.

Title Page

Abstract

Introduction

Conclusions

References

Tables

Figures



Back

Close

Full Screen / Esc

Printer-friendly Version

Interactive Discussion



were mapped based on the method presented in Still et al. (2003). Pixels with barren land and urban areas were reassigned to the bare soil class. Figure 1 shows the 500 m-resolution PFT map for NA.

2.2 Digital elevation model

The HYDRO1k digital elevation model (DEM) for NA was used to generate elevation data. The HYDRO1k is a comprehensive and consistent geographic database providing global coverage of topographically derived data sets such as elevation, slope, aspect, flow accumulation raster layers, and stream lines vector layers. All raster data sets were generated from the USGS 30 arc-second global digital elevation model (GTOPO30) at 1 km resolution, and covered all global landmasses with the exception of Antarctica and Greenland (<http://eros.usgs.gov/>). Compared to other existing global-scale elevation datasets such as the 90 m DEM of the Shuttle Radar Topography Mission (SRTM) (<http://www2.jpl.nasa.gov/srtm/>) and the Advanced Spaceborne Thermal Emission and Reflection Radiometer (ASTER) 30 m Global Digital Elevation Model (GDEM) (<http://asterweb.jpl.nasa.gov/>), HYDRO1k DEM has more complete global coverage and its resolution is closer to existing global-scale land cover data such as the MODIS land cover product. Therefore, it has been widely used in continental and global hydrologic and land surface modelling and was also selected in our study. For consistency with the PFT map, the elevation raster layer for North America was bilinearly interpolated to 500 m resolution (Fig. 2). We excluded Greenland from our study because HYDRO1k does not cover this area.

2.3 Optimal Subgrid Classification (SGC) method of elevation and vegetation

The Subgrid Classification (SGC) method developed in our study considered the joint distribution of elevation and vegetation. Within each model grid (e.g. at resolution $0.1^\circ \times 0.1^\circ$), the SGC method first classified surface elevation from the 500 m DEM data into a limited number of elevation bands (or classes) of equal elevation range. A minimum

Title Page

Abstract

Introduction

Conclusions

References

Tables

Figures

⏪

⏩

◀

▶

Back

Close

Full Screen / Esc

Printer-friendly Version

Interactive Discussion



Enhancing the subgrid land surface representation in land surface models

Y. Ke et al.

Title Page

Abstract

Introduction

Conclusions

References

Tables

Figures

⏪

⏩

◀

▶

Back

Close

Full Screen / Esc

Printer-friendly Version

Interactive Discussion

area threshold of 1 % was used to limit the area of each elevation band. That is, an elevation band containing less than 1 % of the land area of the model grid is added to the neighboring elevation band so that each elevation band covers at least 1 % of the grid land area. Within each elevation band in each model grid, the area was further classified into a limited number of PFTs. For example, if the subgrid surface elevation within a model grid was divided into M elevation bands and the vegetation within each elevation band was classified into N PFTs, the model grid was represented with a total number of $M \times N$ subgrid classes, with each elevation-PFT class treated as a computational unit in the land surface model.

To reduce computational burden, we set the maximum-allowed total number of subgrid classes to “ N_class ” (e.g. 18 classes) for each model grid. The number of elevation bands M and the number of PFTs N for each elevation band are variable for each model grid but $M \times N$ should not exceed the maximum-allowed number N_class (e.g. 18). Hence the combination of M and N is variable and is chosen to best represent the subgrid variability of both PFT and elevation. For example, for a total of 18 maximum-allowed subgrid classes ($N_class = 18$), possible combinations include 3 elevation bands and 6 PFTs per elevation band, or 2 elevation bands and 9 PFTs per elevation band, etc., but the optimal combination was selected. Two criteria must be satisfied for the optimal classification: (1) the elevation range of each elevation band is less than and close to 100 m; and (2) total percentage of subgrid PFTs correctly classified by the method is no less than 80 % for each model grid. We prioritized criteria (2) so that if none of the combinations satisfies both conditions, the classification explaining more than 80 % of PFTs and with elevation range greater than but closest to 100 m was selected; if more than one combination satisfy both conditions, the classification that correctly classifies the most subgrid PFTs was selected.

2.4 SGC method evaluation

In CLM 4.0, vegetation was represented as the composition of 15 PFTs plus bare soil. The simplest and least computationally intensive way to incorporate elevation

distribution of vegetation is to assign a single elevation band to each PFT within a model grid, that is, the surface elevation in the area covered by each PFT was aggregated to one elevation band. We used this method as a baseline to assess the performance of the SGC method with similar computational burden at different model resolutions.

The SGC method was also evaluated by comparing it with two other subgrid classification methods based on a fixed number of elevation bands and vegetation types. The first subgrid classification method (SGC1) was the *M elevation bands-N PFTs* method. Each model grid cell is first divided into *M* equal-interval elevation bands and each elevation band was further classified into *N* PFTs. The second subgrid classification method (SGC2) was the *N PFTs-M elevation bands* method. Each model grid cell was first classified into *N* PFTs and the area covered by each PFT was further divided into *M* equal-interval elevation bands. For both methods, we used the minimum area threshold of 1% to restrict the number of elevation bands in the same way that was used in the SGC method. The SGC1 and SGC2 methods take different perspectives of topographic-vegetation distribution in that SGC1 examines the PFT distribution at different elevation bands and SGC2 examines the elevation distribution of each PFT. However, both methods classify the model grids into fixed numbers of elevation bands and PFTs and the total number of classes is $M \times N$ per model grid throughout the study area.

We implemented the classification methods SGC, SGC1 and SGC2 in North America at 0.1° , 0.25° , 0.5° , 1.0° , and 2.0° resolution with different combinations of number of elevation bands and vegetation types: (1) *Scheme 1*: $N_{\text{class}} = 24$, $M = 6$, $N = 4$, meaning 24 maximum-allowed classes for the SGC method and the combination of 6 elevation bands and 4 PFTs for the SGC1 and SGC2 methods; (2) *Scheme 2*: $N_{\text{class}} = 18$, $M = 6$, $N = 3$; and (3) *Scheme 3*: $N_{\text{class}} = 12$, $M = 4$, $N = 3$. The baseline subgrid method was also implemented at the five resolutions. The three schemes represent different computational burdens with Scheme 1 being most computationally intensive because it has the largest number of total subgrid classes for each model grid.

GMDD

6, 2177–2212, 2013

Enhancing the subgrid land surface representation in land surface models

Y. Ke et al.

Title Page

Abstract

Introduction

Conclusions

References

Tables

Figures



Back

Close

Full Screen / Esc

Printer-friendly Version

Interactive Discussion

Enhancing the subgrid land surface representation in land surface models

Y. Ke et al.

Title Page

Abstract

Introduction

Conclusions

References

Tables

Figures



Back

Close

Full Screen / Esc

Printer-friendly Version

Interactive Discussion



Spatial and statistical comparisons of the three methods at different model resolutions and with different vegetation/elevation combinations were performed in order to compare their abilities to explain the joint distributions of both vegetation and elevation. Generally, the total percentage of PFTs explained within each model grid was used to measure the method's ability to characterize subgrid vegetation; the mean standard deviation of elevation averaged over all elevation bands σ_{ep} (Eqs. 1, 2) within each model grid and the mean elevation interval for all elevation bands l_{ep} (Eqs. 3, 4) were used to measure how well the method describes the subgrid variability of topography.

For the SGC and SGC1 methods, σ_{ep} at a given model grid was calculated as:

$$\sigma_{ep} = \frac{1}{N_b} \sum_{i=1}^{N_b} \sigma_{eb}(i) \quad (1)$$

where $\sigma_{eb}(i)$ is the standard deviation of subgrid surface elevation within the i -th elevation band, and N_b is the number of elevation bands in that grid.

For the baseline and SGC2 methods, σ_{ep} was calculated as:

$$\sigma_{ep} = \frac{1}{N_p} \sum_{j=1}^{N_p} \left[\frac{1}{N_b} \sum_{i=1}^{N_b} \sigma_{eb}(i, j) \right] \quad (2)$$

where $\sigma_{eb}(i, j)$ is the standard deviation of subgrid surface elevation within the i -th elevation band for the j -th dominant PFT, and N_p is the number of dominant PFTs in that grid. For the baseline method, N_p can be any number within 16 because all PFTs within each model grid were included, and N_b equals to 1 because only one elevation band was assigned to each PFT.

Similarly, for the SGC and SGC1 methods, l_{ep} at a given model grid was calculated as:

$$l_{ep} = \frac{1}{N_b} \sum_{i=1}^{N_b} l_{eb}(i) \quad (3)$$

where $l_{\text{eb}}(i)$ is the elevation interval for the i -th elevation band, which is calculated as the difference between the maximum and minimum elevation within the i -th elevation band.

For the baseline and SGC2 methods, l_{ep} was calculated as:

$$l_{\text{ep}} = \frac{1}{N_P} \sum_{j=1}^{N_P} \left[\frac{1}{N_b} \sum_{i=1}^{N_b} l_{\text{eb}}(i, j) \right] \quad (4)$$

where $l_{\text{eb}}(i, j)$ is the elevation interval within the i -th elevation band for the j -th PFT. In the next section, the spatial distributions of the percentage of PFTs explained by the method and σ_{ep} were visually examined; the average percentage of PFTs explained and average σ_{ep} and l_{ep} across NA and their standard deviations were also compared.

3 Results and discussions

3.1 The SGC method

Figure 3 shows the number of PFTs and the average standard deviation of elevation for all PFTs (σ_{ep} , Eq. 2) from the baseline subgrid classification method over the NA continent at 0.1° and 1.0° resolutions. At both spatial resolutions, more PFT classes per grid, i.e. greater subgrid variability of vegetation is found in the coastal areas (over 5 PFTs) than in the inland region such as the Great Plains (1–2 PFTs at 0.1° resolution) where crop dominates the landscape. Increasing model grid size results in greater subgrid-scale variability of PFTs (Fig. 3a, b). When assigning one elevation band to each PFT within the model grid, σ_{ep} shows substantial spatial variance across the continent (Fig. 3c, d). It is evident that the spatial distribution of σ_{ep} corresponds with topographic variations. In western NA with complex topography such as the Coastal Range and Rocky Mountains, σ_{ep} is larger than in flat areas such as the Great Plains and coastal area in southeast NA. The spatial contrast becomes more distinct at coarser

Enhancing the subgrid land surface representation in land surface models

Y. Ke et al.

Title Page

Abstract

Introduction

Conclusions

References

Tables

Figures

⏪

⏩

◀

▶

Back

Close

Full Screen / Esc

Printer-friendly Version

Interactive Discussion

resolution as the subgrid topographic variability becomes larger. In the western NA, σ_{ep} is above 200 m and reaches 1000 m, while σ_{ep} decreases to below 30 m in the Great Plains at 1.0° resolution. The average σ_{ep} across the continent rapidly increases from 43.1 m at 0.1° resolution to 59.1 m at 0.25° resolution, 76.0 m at 0.5° resolution, 94.8 m at 1.0° resolution, and 119.3 m at 2.0° resolution, indicating that with the baseline method, substantially less subgrid topographic details are represented at coarser resolution.

Compared to the baseline method where the number of PFTs and the number of elevation band per PFT were pre-determined, the optimal SGC method produced much more spatially variant number of elevation bands and number of PFTs within each elevation band throughout the continent (Figs. 4a, b, 5a, b, and 6a, b). With comparable number of total classes (15 classes for the baseline method and $N_{class} = 18$ for the SGC method), the SGC method substantially suppresses σ_{ep} especially in topography-complex areas (Fig. 3c vs. Fig. 5d, Fig. 3d vs. Fig. 6d), indicating that greater detail of subgrid topography was described by the SGC method. The advantage of the SGC method over the baseline method in explaining elevation variability is more prominent at coarser resolution (Fig. 3d vs. Fig. 6d) as σ_{ep} is generally less than 60 m for the SGC method in the Pacific Northwest (Fig. 6d) compared to over 200 m for the baseline method (Fig. 3d). However, more detailed elevation information in the SGC method compromises the representation of PFTs compared to the baseline method that considers all PFTs within each model grid. Nevertheless, the SGC method still explained a reasonable amount of PFT variability (over 80 % in Figs. 5c, 6c) while greatly improving the elevation variability, which has equally if not larger impacts on land surface processes as PFT variability (Leung and Ghan, 1998), at computational cost comparable to the baseline method.

The comparison between different N_{class} (Figs. 4b, 5b) and varying model resolutions (Figs. 5b, 6b) shows that both the number of elevation bands and number of PFTs demonstrate similar spatial pattern in North America. In the areas with more complex topography such as the Coastal Range, Rocky Mountains, and Appalachian

Enhancing the subgrid land surface representation in land surface models

Y. Ke et al.

Title Page

Abstract

Introduction

Conclusions

References

Tables

Figures



Back

Close

Full Screen / Esc

Printer-friendly Version

Interactive Discussion

Mountains (Fig. 2), the SGC method generated substantially more elevation bands than in flat areas such as the Central and Coastal Plains (Figs. 3b, 4b, 5b). The spatial distribution of the number of PFTs within each elevation band, on the other hand, generally shows an opposite pattern (Figs. 3a, 4a, 5a). In western NA where more elevation bands were generated, smaller numbers of PFTs within each elevation bands were produced because the combined number of PFTs and elevation bands was restricted by N_{class} . Still, the total PFTs explained by the method was over 80 % for each model grid (Figs. 4c, 5c, 6c) because driven by climate, PFT is more correlated with elevation in over complex terrains. This allows the SGC method to optimally represent subgrid variations in both topography and vegetation. In the flat areas of central and eastern NA, more than six PFTs were generated that explained over 98 % of the total PFTs in the model grids. In the Great Plains, only one to two elevation bands and no more than two PFTs within each elevation band were generated for the flat terrain and cropland-dominated landscape.

To assess the impacts of N_{class} , we note from Figs. 4d and 5d that 24 total classes reduced the mean standard deviations of elevation averaged from all elevation bands in western NA compared to 18 total classes because finer elevation intervals afforded by using a larger number of elevation bands yield more detailed representation of topographic relief. However, decreasing N_{class} does not considerably influence the number of PFTs per elevation band (Figs. 4a, 5a) at 0.1° resolution. Reducing model resolution from 0.1° to 1.0° resulted in generally more elevation bands and more PFTs per elevation band because the model grids encompass greater subgrid variability of vegetation and topography.

Figure 7 illustrates that the average number of elevation bands, number of PFTs per band, and the number of total classes generated by the SGC method show similar increasing trends with decreasing model resolutions and increasing number of N_{class} . At the finest resolution of 0.1° , the average number of total classes increases only slightly with increasing N_{class} (6 for N_{class} of 12, 7 for N_{class} of 18, and 7.9 for N_{class} of 24), because the low subgrid variability within a small grid cell can be well

Enhancing the subgrid land surface representation in land surface models

Y. Ke et al.

Title Page

Abstract

Introduction

Conclusions

References

Tables

Figures

⏪

⏩

◀

▶

Back

Close

Full Screen / Esc

Printer-friendly Version

Interactive Discussion



represented by a small number of subgrid classes. At resolution of 2° , the average number of total classes increases to 10.2, 15.2, and 20, for N_{class} equals 12, 18, and 24, respectively. As the subgrid topography and vegetation variation increase with coarser model resolution, more classes are required to explain a reasonable amount of topography and vegetation variations and the method is more restricted by the maximum-allowed number of classes. This is consistent with what can be seen in Fig. 8, which shows the spatial distribution of the actual number of classes generated from the SGC method. At 0.1° model grid size, changing N_{class} does not significantly change the number of classes except in western NA with complex topography. At 1° resolution, the number of classes decrease dramatically with decreasing N_{class} throughout the NA continent. There is no distinct difference between the flat areas and the topographically-complex areas especially when N_{class} is 12. These show the method's ability in assigning optimal classes for different model resolutions and a larger number of maximum-allowed total classes gives more flexibility in assigning the best suitable combination of elevation bands and PFTs.

Comparison of Fig. 7a and c indicates that the increase in the number of total classes is mainly attributed to the increase in the number of elevation bands as both metrics show similar trend. In contrast, the average number of PFTs per elevation band increases more slowly, and can even decrease with increasing model grid size. For example, on average 3.3 PFTs are produced within each elevation band at 1° resolution ($N_{\text{class}} = 12$ in Fig. 7b), but only 3.1 PFTs are needed for each elevation band at 2° resolution ($N_{\text{class}} = 12$ in Fig. 7b) to explain at least 80% of total PFTs. This indicates that the subgrid variability of surface elevation changes more dramatically than the subgrid variability of vegetation type with changing model resolution and highlights the importance of considering the topographic distribution of vegetation types.

3.2 Comparison of three subgrid classification methods

The optimal subgrid classification method SGC was evaluated against the SGC1 and SGC2 methods with fixed number of elevation bands and PFTs. Figure 9a shows that

Enhancing the subgrid land surface representation in land surface models

Y. Ke et al.

Title Page

Abstract

Introduction

Conclusions

References

Tables

Figures

⏪

⏩

◀

▶

Back

Close

Full Screen / Esc

Printer-friendly Version

Interactive Discussion

all three methods explained a large fraction of total PFTs above 94 %. The percentage of PFTs represented by each method, when averaged across the NA continent, decreases with increasing model grid size and decreasing number of elevation bands M or PFTs N (Fig. 9a). The standard deviation of the percentage PFTs explained across the NA continent increases with increasing model grid size and decreasing M and N (Fig. 9b). With $M = 6$, $N = 4$ and $N_{\text{class}} = 24$, the SGC1 method, which first classifies topography into 6 elevation bands and represents each elevation band with 4 most dominant PFTs explains the most PFTs, while the optimal classification method produced the lowest percentage of PFTs except at 0.1° resolution.

The spatial distribution of the differences in the percentage of PFT explained (Fig. 10a, d) illustrates that areas with less PFTs explained by the SGC method (negative values of SGC-SGC1 or SGC-SGC2) mainly concentrate in the mountainous western NA with complex topography. The SGC method explains 2–15 % less PFTs than the other two methods. In these areas, the SGC method required more elevation bands to represent reasonable variations of elevation (e.g. over 10 elevation bands were produced in these areas in Fig. 4b), thus sacrificing the total PFTs represented (only 2–3 PFTs were identified in this area in Fig. 4a compared to four PFTs used in SGC1 and SGC2 methods). Despite the lower amount of PFTs explained in the western NA, more PFTs are explained by the SGC method than the other two methods in the south-east United States such as Florida, Mississippi, South Carolina and Georgia, and in central Canada where the SGC method identified more than four PFTs because few elevation classes are needed to represent the flat topography. When fewer PFTs were used in SGC1 and SGC2 and fewer N_{class} was used in SGC, the areas of positive difference in the percentage of PFT explained between SGC and the other two methods expanded from central Canada to Alberta and Saskatchewan provinces in western Canada (Fig. 10b, e). In Mexico and central America with distinct topographic relief, SGC explained considerably higher percentage of PFT than SGC2. This emphasizes the advantages of considering topographic distributions of vegetation in topography-complex and species-rich areas because vegetation type correlates with topography.

Enhancing the subgrid land surface representation in land surface models

Y. Ke et al.

Title Page

Abstract

Introduction

Conclusions

References

Tables

Figures

⏪

⏩

◀

▶

Back

Close

Full Screen / Esc

Printer-friendly Version

Interactive Discussion

With 18 maximum-allowed number of total classes in the SGC method, $M = 6$ and $N = 3$, the negative differences in PFTs between SGC and the other two methods were compensated by positive differences (Fig. 10b, e). Hence overall, the average percentage of PFTs explained by SGC is higher than the other two methods across all resolutions (Fig. 9a). As N_{class} decreases to 12, at the finest resolution of 0.1° , SGC explained slightly greater percentage of PFTs than the other methods. With this computational burden, as model grid size increases the performance of SGC decreases rapidly as indicated by the rapid decrease in the percentage PFTs explained (Fig. 9a) and increase in the standard deviation of PFTs (Fig. 9b). At the resolution of 1° or higher, SGC explained lower amount of PFTs than the other two methods. As stated above, at coarse resolution SGC is more restricted by the number of maximum-allowed classes because larger variations of PFTs and topography exist. Since topography shows more distinct change than PFTs (Fig. 7a, b), the balance between the number of elevation bands and PFTs resulted in less PFTs explained by the method.

Although the SGC method shows varying performances in terms of the average percent of PFTs explained compared to the other two methods, the PFTs explained by this method is more spatially homogeneous – all model grids in the study area have over 80 % of total PFTs explained regardless of N_{class} and model resolution. In contrast, the PFTs explained by SGC1 and SGC2 can be as low as 52 % (Fig. 9c), and around 92.7 % of the model grids have over 80 % of the PFTs explained (Fig. 9d).

The abilities of the three methods in explaining topographic variation were shown in Fig. 11. For all three methods, the average standard deviation of elevation σ_{ep} for all elevation bands increase with model grid size. Since σ_{ep} indicates the subgrid variation of elevation within each elevation band, smaller value of average σ_{ep} means better overall representation of subgrid topography, and vice versa. It is apparent that classifying the surface elevation into a limited number of elevation bands greatly reduce the standard deviation of elevation represented in the model grids; for example, the average standard deviation of elevation within the model grids varies from 59.1 m to 119.3 m from

0.1° to 1° resolution for the baseline method, while the average σ_{ep} substantially decreased and the ranges narrow down to 9.4 from 63.4 (Fig. 10a) for the SGC method.

At fine resolutions from 0.1° to 0.5°, the average σ_{ep} from the SGC method with N_{class} of 24 (and 18) is greater than the SGC1 and SGC 2 methods with $M = 6$ and $N = 4$ (and $N = 3$) (Fig. 11a), meaning that SGC1 and SGC2 have better overall representation of elevation variability at these scales. When model resolution decreases, the advantage of the SGC method in elevation representation emerges. At both 1° and 2° resolutions, the average σ_{ep} from SGC is lower than that from SGC1 and SGC2. Comparison of the spatial distribution of σ_{ep} in Fig. 12 shows that at both fine and coarse resolutions, the SGC method produced distinctly lower σ_{ep} in western NA and the Appalachian Mountains region than the other two methods, as the number of elevation bands in these areas increased (over 6 in Figs. 4b, 5b, 6b). Although σ_{ep} in flat areas from SGC is slightly greater than that from the other two methods, SGC is still able to produce reasonable representation of elevation variability as σ_{ep} is less than 30 m in these areas (Figs. 3d, 4d, 5d). This implies that using 6 or 4 elevation bands may be redundant in these areas because topography does not vary much and vegetation distribution has little relation to topography.

Compared to those from SGC1 and SGC2, the average σ_{ep} from SGC climbs more slowly with increasing model grid size and decreasing number of maximum-allowed classes. For example, the average σ_{ep} from SGC with 24 N_{class} ranges from 16.2 to 30.2 across resolutions from 0.1° to 2°, while SGC2 with 4 PFTs and 6 elevation bands within each PFT-covered area produced average σ_{ep} from 9.4 to 38.6, and SGC1 produced even larger range of average σ_{ep} from 11.1 to 46.9. The average elevation interval I_{ep} shows similar pattern (Fig. 11c). Because topography shows much greater variability at coarser scales, the slower change in average σ_{ep} indicates more stable performance of the SGC method across different scales.

Although the average σ_{ep} from SGC is higher than that from the other methods at fine resolution (e.g. less than 1°), the variation of σ_{ep} across NA is smaller than that from the other two methods (Fig. 11b) at each model resolution and with each scheme of

GMDD

6, 2177–2212, 2013

Enhancing the subgrid land surface representation in land surface models

Y. Ke et al.

Title Page

Abstract

Introduction

Conclusions

References

Tables

Figures



Back

Close

Full Screen / Esc

Printer-friendly Version

Interactive Discussion



Enhancing the subgrid land surface representation in land surface models

Y. Ke et al.

Title Page

Abstract

Introduction

Conclusions

References

Tables

Figures

⏪

⏩

◀

▶

Back

Close

Full Screen / Esc

Printer-friendly Version

Interactive Discussion

computational burden. This means that the elevation variability explained by the SGC method is more spatially homogeneous than the other two methods. The SGC method adjusts the number of elevation bands flexibly to ensure that the elevation range within each elevation band for each model grid is less than and close to 100 m at the premise of over 80 % PFTs explained in the model grid. Therefore more elevation bands were produced in complex terrain than in flat land surface. In contrast, SGC1 and SGC2 represent the subgrid elevation in each model grid by a fixed number of elevation bands regardless of the land surface topography. Hence they can produce very small σ_{ep} in flat area but large σ_{ep} in mountainous regions. The spatial homogeneity of the SGC method is also noted in Fig. 11d. At the same resolution and with the same computational burden, there are more model grids with less than 100 m average elevation interval per elevation band from the SGC method than those from the other methods. For example, using the SGC method, over 80 % of the grid cells have less than 100 m elevation range within the elevation bands even at 2° resolution ($N_{class} = 24$), while with the same computational burden the percentage of grids decreases to 54 % for SGC1 and 47 % for SGC2 ($M = 6$, $N = 4$).

The combined examination of Figs. 9–12 and the statistical analysis in Table 1 show that the SGC method is not necessarily superior to the other two methods in terms of both vegetation and elevation variation explained, when a large number of subgrid classes is allowed ($N_{class} = 24$). However, when computational burden is moderately alleviated using fewer number of subgrid classes ($N_{class} = 18$, $M = 6$ and $N = 3$), the SGC method begins to demonstrate its advantage in balancing the variability of vegetation and elevation distribution that can be explained. At the coarser resolutions of 1° to 2°, the SGC method becomes clearly superior to both SGC1 and SGC2, i.e. a statistically greater percentage of PFTs was explained and σ_{ep} is smaller. With N_{class} of 12, the SGC method is better than SGC2 at the resolutions of 0.5° or coarser and better than SGC1 only at the resolution of 0.25°.

4 Conclusions

In this study we presented a new subgrid method to enhance the representation of land surface characteristics in land surface models. Built on the current subgrid structure of CLM that defines subgrid fractional area of multiple PFTs, the method incorporates topographic distributions of PFTs. For each model grid, the method assigned variable elevation and vegetation classes based on their joint distribution so that the subgrid-scale variability of both can be explained in an optimal and computationally efficient manner. Compared to the baseline method, which assigns a single elevation class to each PFT, the new method provides an obvious advantage in representing topographic variability at a similar computational efficiency as the average standard deviation of surface elevation in each elevation band was greatly suppressed. Although this compromised the ability to represent vegetation variability compared to the baseline method, the new method still explained at least 80 % of the total PFTs in each model grid. The effectiveness of the new method in representing subgrid variability in both topography and vegetation is partly related to the correlation between topography and vegetation. However, this effectiveness decreases with decreasing model resolution because the elevation dependence of vegetation is weaker at coarser spatial scales.

Compared to the other subgrid approaches with pre-determined number of elevation classes and vegetation types (SGC1 and SGC2), the new method presented in this study assigned variable number of elevation and vegetation classes to balance the representation of both topography and vegetation variability under the restriction of a maximum-allowed number of total classes. Among the three schemes with different computational burdens, the new method shows advantages over the other methods with moderate computation intensity and at coarse scales in that both PFTs and topography variability was best explained. Furthermore, the variability of both vegetation and elevation explained by the new method was more spatially homogeneous compared to the SGC1 and SGC2 methods regardless of model resolutions and computational burdens.

Enhancing the subgrid land surface representation in land surface models

Y. Ke et al.

Title Page

Abstract

Introduction

Conclusions

References

Tables

Figures



Back

Close

Full Screen / Esc

Printer-friendly Version

Interactive Discussion



Enhancing the subgrid land surface representation in land surface models

Y. Ke et al.

Title Page

Abstract

Introduction

Conclusions

References

Tables

Figures

⏪

⏩

◀

▶

Back

Close

Full Screen / Esc

Printer-friendly Version

Interactive Discussion

Spatial heterogeneity of surface cover and topography has important control on many land processes. This study assessed different methods to classify the subgrid spatial distribution of surface cover and topography. When implemented in the model, the fractional area of each elevation band and PFT can be determined and the mean elevation of each elevation band can be defined. Separate calculations of surface processes can be performed for each class, and the output fluxes at each class can then be aggregated in an area-weighted manner for each grid cell. To maximize the benefits of representing both subgrid PFT and topography on land surface and coupled land-atmosphere simulations, subgrid atmospheric forcings such as temperature, precipitation, and radiation should be provided to account for the important influence of topography on atmospheric processes. Subgrid parameterizations such as Leung and Ghan (1998) to represent the subgrid topographic influence on precipitation or simple lapse rate based adjustment of temperature and precipitation (e.g. Liang et al., 1994) should be explored. The impacts of the new subgrid classification on land surface simulations at different model resolutions will be studied in the future.

Acknowledgements. The authors acknowledge the Pacific Northwest National Laboratory (PNNL) Platform for Regional Integrated Modeling and Analysis (PRIMA) Initiative, which supported the development of databases used in the study, and the Climate Science for Sustainable Energy Future (CSSEF) project funded by the Department of Energy (DOE) Earth System Modeling program, which supported the development and analysis of various subgrid classification methods. PNNL is operated by Battelle for the DOE under Contract DE-AC06-76RLO 1830. The first author also acknowledges the support from the Key Program of National Natural Science Foundation of China (NSFC) (41130744/D0107), the General Program of NSFC (41171335/D010702), and the 973 Program of China (2012CB723403).

References

Barbour, M. G., Burk, J. H., and Pitts, W. D.: Terrestrial Plant Ecology, 3rd Edn., Benjamin/Cummings, Publishing Co., Menlo Park, California, 688 pp., 1998.

Enhancing the subgrid land surface representation in land surface models

Y. Ke et al.

Title Page

Abstract

Introduction

Conclusions

References

Tables

Figures

⏪

⏩

◀

▶

Back

Close

Full Screen / Esc

Printer-friendly Version

Interactive Discussion

- Bonan, G. B., Levis, S., Kergoat, L., and Oleson, K. W.: Landscapes as patches of plant functional types: an integrating concept for climate and ecosystem models, *Global Biogeochem. Cy.*, 16, 5-1–5-23, doi:10.1029/2000GB001360, 2002a.
- Bonan, G. B., Oleson, K. W., Vertenstein, M., Levis, S., Zeng, X., Dai, Y., Dickinson, R. E., and Yang, Z. L.: The land surface climatology of the Community Land Model coupled to the NCAR Community Climate Model, *J. Climate*, 15, 3123–3149, doi:10.1175/1520-0442(2002)015<3123:TLSCOT>2.0.CO;2, 2002b.
- Brown, D. G.: Predicting vegetation types at treeline using topography and biophysical disturbance variables, *J. Veg. Sci.*, 5, 641–656, doi:10.2307/3235880, 1994.
- Ek, M. B., Mitchell, K. E., Lin, Y., Rogers, E., Grunmann, P., Koren, V., Gayno, G., and Tarp-
ley, J. D.: Implementation of Noah land surface model advances in the National Centers for Environmental Prediction operational mesoscale Eta model, *J. Geophys. Res.*, 108, D228851, doi:10.1029/2002JD003296, 2003.
- Ghan, S. J., Liljegren, J. C., Shaw, W. J., Hubbe, J. H., and Doran, J. C.: Influence of subgrid variability on surface hydrology, *J. Climate*, 10, 3157–3166, 1996.
- Ghan, S. J., Shippert, T. R., and Fox, J.: Physically based global downscaling: regional evaluation, *J. Climate*, 19, 429–445, doi:10.1175/JCLI3622.1, 2006.
- Giorgi, F. and Avissar, R.: Representation of heterogeneity effects in earth system modeling: experience from land surface modeling, *Rev. Geophys.*, 35, 413–437, doi:10.1029/97RG01754, 1997.
- Giorgi, F., Francisco, R., and Pal, J.: Effects of a subgrid-scale topography and land use scheme on the simulation of surface climate and hydrology, Part I: Effects of temperature and water vapor disaggregation, *J. Hydrometeorol.*, 4, 317–333, doi:10.1175/1525-7541(2003)4<317:EOASTA>2.0.CO;2, 2003.
- Hijmans, R. J., Cameron, S. E., Parra, J. L., Jones, P. G., and Jarvis, A.: Very high resolution interpolated climate surfaces for global land areas, *Int. J. Climatol.*, 25, 1965–1978, doi:10.1002/joc.1276, 2005.
- Ke, Y., Leung, L. R., Huang, M., Coleman, A. M., Li, H., and Wigmosta, M. S.: Development of high resolution land surface parameters for the Community Land Model, *Geosci. Model Dev.*, 5, 1341–1362, doi:10.5194/gmd-5-1341-2012, 2012.
- Koster, R. D. and Suarez, M. J.: A comparative analysis of two land surface heterogeneity representations, *J. Climate*, 5, 1379–1390, doi:10.1175/1520-0442(1992)005<1379:ACAOTL>2.0.CO;2, 1992.

Enhancing the subgrid land surface representation in land surface models

Y. Ke et al.

Title Page

Abstract

Introduction

Conclusions

References

Tables

Figures

⏪

⏩

◀

▶

Back

Close

Full Screen / Esc

Printer-friendly Version

Interactive Discussion

- Krinner, G., Viovy, N., de Noblet-Ducoudré, N., Ogée, J., Polcher, J., Friedlingstein, P., Ciais, P., Sitch, S., and Prentice, I. C.: A dynamic global vegetation model for studies of the coupled atmosphere-biosphere system, *Global Biogeochem. Cy.*, 19, GB1015, doi:10.1029/2003GB002199, 2005.
- 5 Krinner, G., Lezine, A.-M., Braconnot, P., Sepulchre, P., Ramstein, G., Grenier, C., and Gouttevin, I.: A reassessment of lake and wetland feedbacks on the North African Holocene climate, *Geophys. Res. Lett.*, 39, L07701, doi:10.1029/2012GL0500992, 2012.
- Lawrence, D., Oleson, K. W., Flanner, M. G., Thornton, P. E., Swenson, S. C., Lawrence, P. J., Zeng, X., Yang, Z. L., Levis, S., and Sakaguchi, K.: Parameterization improvements and functional and structural advances in version 4 of the Community Land Model, *J. Adv. Model. Earth Syst.*, 3, M03001, doi:10.1029/2011MS000045, 2011
- 10 Lawrence, P. J. and Chase, T. N.: Representing a new MODIS consistent land surface in the Community Land Model (CLM 3.0), *J. Geophys. Res.*, 112, G01023, doi:10.1029/2006JG000168, 2007.
- 15 Leung, L. R. and Ghan, S. J.: A subgrid parameterization of orographic precipitation, *Theor. Appl. Climatol.*, 52, 95–118, doi:10.1007/BF00865510, 1995.
- Leung, L. R. and Ghan, S. J.: Parameterizing subgrid orographic precipitation and surface cover in climate models, *Mon. Weather Rev.*, 126, 3271–3291, doi:10.1175/1520-0493(1998)126<3271:PSOPAS>2.0.CO;2, 1998.
- 20 Leung, L. R., Wigmosta, M. S., Ghan, S. J., Epstein, D. J., and Vail, L. W.: Application of a subgrid orographic precipitation/surface hydrology scheme to a mountain watershed, *J. Geophys. Res.*, 101, 12803–12818, doi:10.1029/96JD00441, 1996.
- Li, H., Wigmosta, M. S., Wu, H., Huang, M., Ke, Y., Coleman, A. M., and Leung, L. R.: A physically based runoff routing model for land surface and earth system models, *J. Hydrometeorol.*, doi:10.1175/JHM-D-12-015.1, in press, 2013.
- 25 Li, R. and Arora, V. K.: Effect of mosaic representation of vegetation in land surface schemes on simulated energy and carbon balances, *Biogeosciences*, 9, 593–605, doi:10.5194/bg-9-593-2012, 2012.
- Liang, X., Lettenmaier, D. P., Wood, E. F., and Burges, S. J.: A simple hydrologically based model of land surface water and energy fluxes for general circulation models, *J. Geophys. Res.*, 99, 14415–14428, 1994.
- 30

Enhancing the subgrid land surface representation in land surface models

Y. Ke et al.

Title Page

Abstract

Introduction

Conclusions

References

Tables

Figures

⏪

⏩

◀

▶

Back

Close

Full Screen / Esc

Printer-friendly Version

Interactive Discussion

- Nijssen, B., Schnur, R., and Lettenmaier, D. P.: Global retrospective estimation of soil moisture using the variable infiltration capacity land surface model, 1980–93, *J. Climate*, 14, 1790–1808, doi:10.1175/1520-0442(2001)014<1790:GREOSM>2.0.CO;2, 2001.
- 5 Niu, G.-Y., Yang, Z.-L., Mitchell, K. E., Chen, F., Ek, M. B., Barlage, M., Kumar, A., Manning, K., Niyogi, D., Rosero, E., Tewari, M., and Xia, Y.: The community Noah land surface model with multiparameterization options (NoahMP): 1. Model description and evaluation with localscale measurements, *J. Geophys. Res.*, 116, D12109, doi:10.1029/2010JD015139, 2011.
- Oleson, K. W. and Bonan, G. B.: The effects of remotely sensed plant functional type and leaf area index on simulations of boreal forest surface fluxes by the NCAR land surface model, *J. Hydrometeorol.*, 1, 431–446, doi:10.1175/1525-7541(2000)001<0431:TEORSP>2.0.CO;2, 2000.
- 10 Oleson, K. W., Lawrence, D. M., Bonan, G. B., Flanner, M. G., Kluzek, E., Lawrence, P. J., Levis, S., Swenson, S. C., Thornton, P. E., Dai, A., Decker, M., Dickinson, R., Feddema, J., Heald, C. L., Hoffman, F., Lamarque, J.-F., Mahowald, N., Niu, G.-Y., Qian, T., Randerson, J., Running, S., Sakaguchi, K., Slater, A., Stockli, R., Wang, A., Yang, Z.-L., Zeng, X., and Zeng, X.: Technical Description of version 4.0 of the Community Land Model (CLM), National Center for Atmospheric Research, Boulder, CO, NCAR/TN-478+STR, 2010.
- Seth, A., Giorgi, F., and Dickinson, R. E.: Simulating fluxes from heterogeneous land surfaces: explicit subgrid method employing the biosphere-atmosphere transfer scheme (BATS), *J. Geophys. Res.*, 99, 18651–18667, doi:10.1029/94JD01330, 1994.
- 20 Sitch, S., Smith, B., Prentice, I. C., Almut Arneeth, Bondeau, A., Cramer, W., Jed O. Kaplan, Levis, S., Lucht, W., Sykes, M. T., Thonicke, K., and Kenevsky, S.: Evaluation of ecosystem dynamics, plant geography and terrestrial carbon cycling in the LPJ dynamic global vegetation model, *Glob. Change Biol.*, 9, 161–185, doi:10.1046/j.1365-2486.2003.00569.x, 2003.
- 25 Still, C., Berry, J. C., Collatz, G. J., and DeFries, R. S.: Global distribution of C3 and C4 vegetation: carbon cycle implications, *Global Biogeochem. Cy.*, 17, 6-1–6-14, doi:10.1029/2001GB001807, 2003.
- Vankat, J. L.: A gradient perspective on the vegetation of Sequoia National Park, California, *Madrono*, 29, 214–220, 1982.

Enhancing the subgrid land surface representation in land surface models

Y. Ke et al.

Title Page	
Abstract	Introduction
Conclusions	References
Tables	Figures
⏪	⏩
◀	▶
Back	Close
Full Screen / Esc	
Printer-friendly Version	
Interactive Discussion	

Table 1. Paired T-test statistics for four classification schemes in terms of total PFT explained and standard deviation of elevation σ_{ep} . Values in bold indicate significant difference between the two classifications on a 95 % confidence level. Positive value in PFTs and negative value in elevation standard deviation means better capability of explaining both PFT and elevation.

Resolution	SGC vs. SGC1		SGC vs. SGC2	
	Percentage of PFTs explained	σ_{ep}	Percentage of PFTs explained	σ_{ep}
<i>N</i> .class = 24, <i>M</i> = 6, <i>N</i> = 4				
0.1°	-0.7*	277.3	47.4	434.8
0.25°	-19.6	24.9	-1.9*	102.1
0.5°	-16.9	-18.2	-7.1	17.7
1.0°	-12.7	-21.5	-7.0	-6.7
2.0°	-8.2	-17.9	-4.5	-11.3
<i>N</i> .class = 18, <i>M</i> = 6, <i>N</i> = 3				
0.1°	106.0	312.4	150.2	464.6
0.25°	27.9	42.5	46.4	111.1
0.5°	8.6	-10.1	19.4	21.6
1.0°	1.4	-18.1	7.6	-4.3
2.0°	0.38*	-15.8	4.4	-9.0
<i>N</i> .class = 12, <i>M</i> = 4, <i>N</i> = 3				
0.1°	49.0	58.7	88.4	205.8
0.25°	3.2	-36.4	19.4	23.6
0.5°	-4.9	-40.9	4.4	-10.9
1.0°	-6.5	-31.4	-1.0*	-15.7
2.0°	-4.6	-21.1	-0.9*	-14.1

* Not significant.



Enhancing the subgrid land surface representation in land surface models

Y. Ke et al.

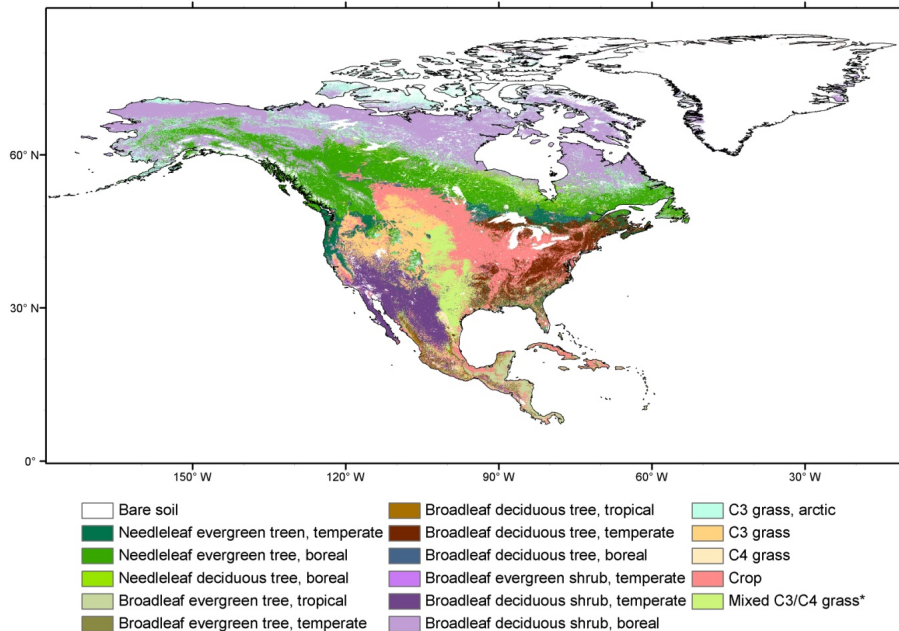


Fig. 1. North America PFT map. *: the area with legend “mixed C3/C4 grass” means the fraction of either C3 or C4 grass in each pixel is less than 1.

Title Page	
Abstract	Introduction
Conclusions	References
Tables	Figures
⏪	⏩
◀	▶
Back	Close
Full Screen / Esc	
Printer-friendly Version	
Interactive Discussion	

Enhancing the subgrid land surface representation in land surface models

Y. Ke et al.

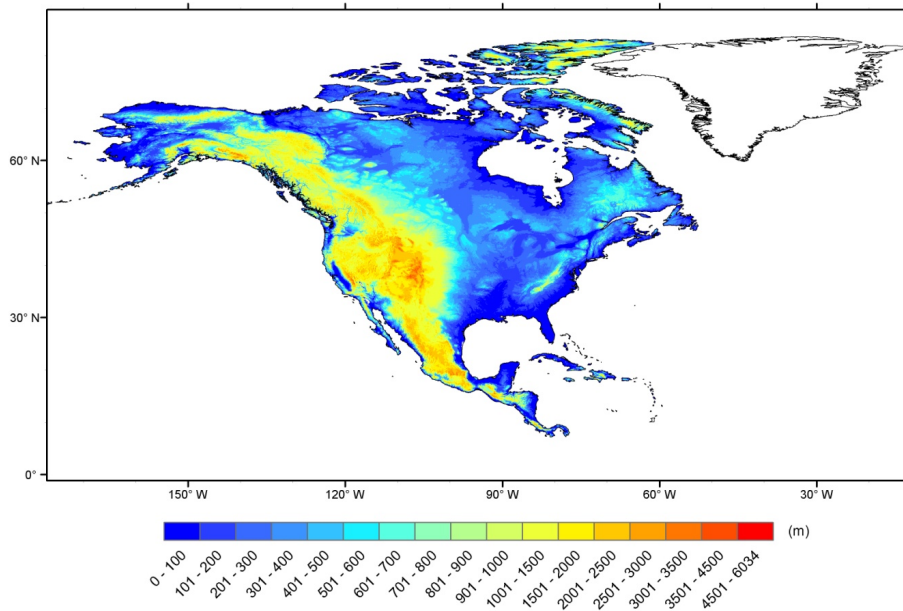


Fig. 2. Elevation distribution in North America.

Title Page	
Abstract	Introduction
Conclusions	References
Tables	Figures
⏪	⏩
◀	▶
Back	Close
Full Screen / Esc	
Printer-friendly Version	
Interactive Discussion	

Enhancing the subgrid land surface representation in land surface models

Y. Ke et al.

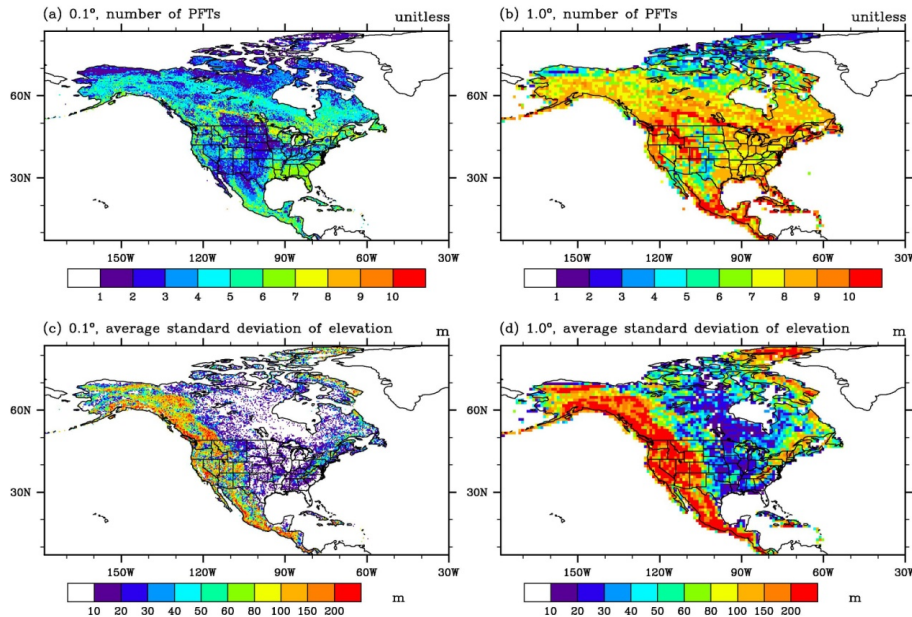


Fig. 3. Baseline subgrid classification method. **(a)** 0.1°, number of PFTs; **(b)** 1.0°, number of PFTs; **(c)** 0.1°, average standard deviation of elevation σ_{ep} ; **(d)** 1.0°, average standard deviation of elevation σ_{ep} .

Title Page

Abstract

Introduction

Conclusions

References

Tables

Figures

⏪

⏩

◀

▶

Back

Close

Full Screen / Esc

Printer-friendly Version

Interactive Discussion

Enhancing the subgrid land surface representation in land surface models

Y. Ke et al.

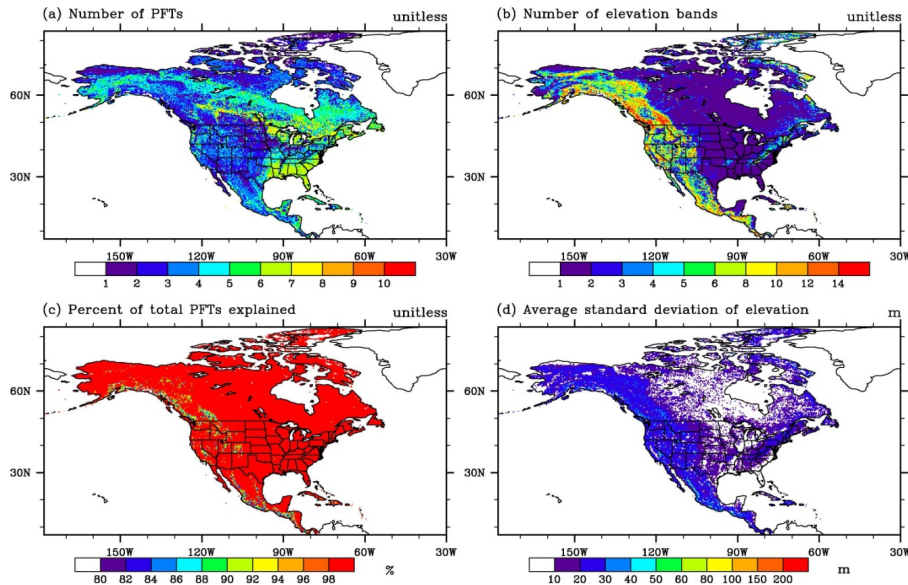


Fig. 4. Optimal classification SGC with maximum-allowed total classes $N_{\text{class}} = 24$ at 0.1° resolution. **(a)** number of dominant PFTs classified for each grid; **(b)** number of elevation bands classified for each grid; **(c)** total percentage of PFTs explained by the method; **(d)** average standard deviation of elevation in each elevation bands in each model grid σ_{ep} .

Title Page

Abstract

Introduction

Conclusions

References

Tables

Figures

⏪

⏩

◀

▶

Back

Close

Full Screen / Esc

Printer-friendly Version

Interactive Discussion

Enhancing the subgrid land surface representation in land surface models

Y. Ke et al.

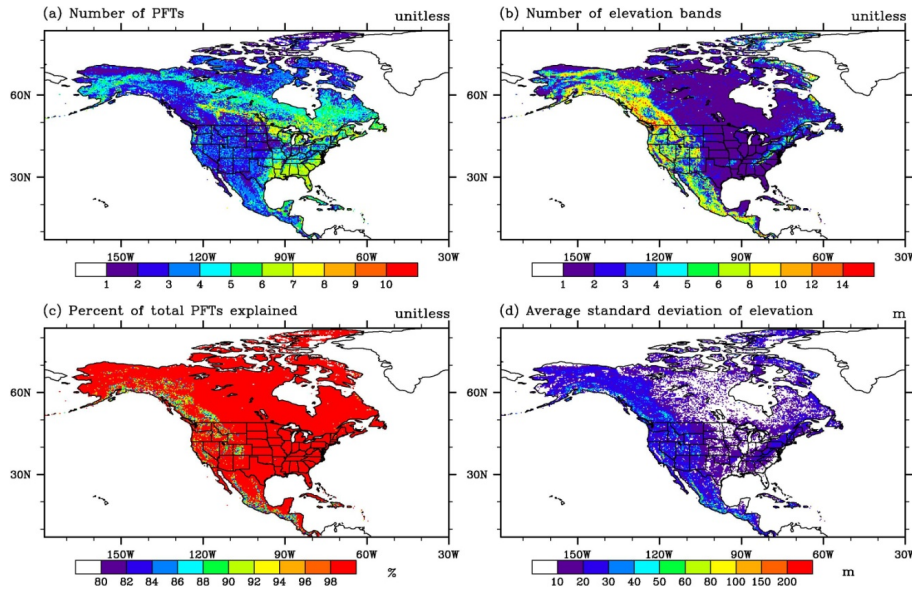


Fig. 5. Optimal classification SGC with maximum-allowed total classes $N_{\text{class}} = 18$ at 0.1° resolution. **(a)** Number of dominant PFTs classified for each grid; **(b)** number of elevation bands classified for each grid; **(c)** total percentage of PFTs explained by the method; **(d)** average standard deviation of elevation in each elevation bands in each model grid σ_{ep} .

Title Page

Abstract

Introduction

Conclusions

References

Tables

Figures

⏪

⏩

◀

▶

Back

Close

Full Screen / Esc

Printer-friendly Version

Interactive Discussion

Enhancing the subgrid land surface representation in land surface models

Y. Ke et al.

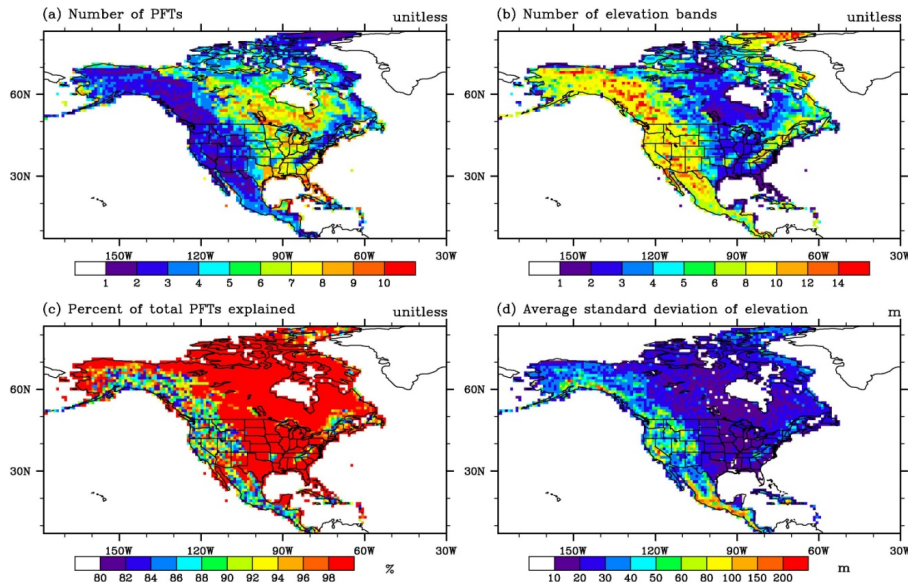


Fig. 6. Optimal classification SGC with maximum-allowed total classes $N_{\text{class}} = 18$ at 1.0° resolution. **(a)** Number of dominant PFTs classified for each grid; **(b)** number of elevation bands classified for each grid; **(c)** total percentage of PFTs explained by the method; **(d)** average standard deviation of elevation in each elevation bands in each model grid σ_{ep} .

Title Page

Abstract

Introduction

Conclusions

References

Tables

Figures



Back

Close

Full Screen / Esc

Printer-friendly Version

Interactive Discussion

Enhancing the subgrid land surface representation in land surface models

Y. Ke et al.

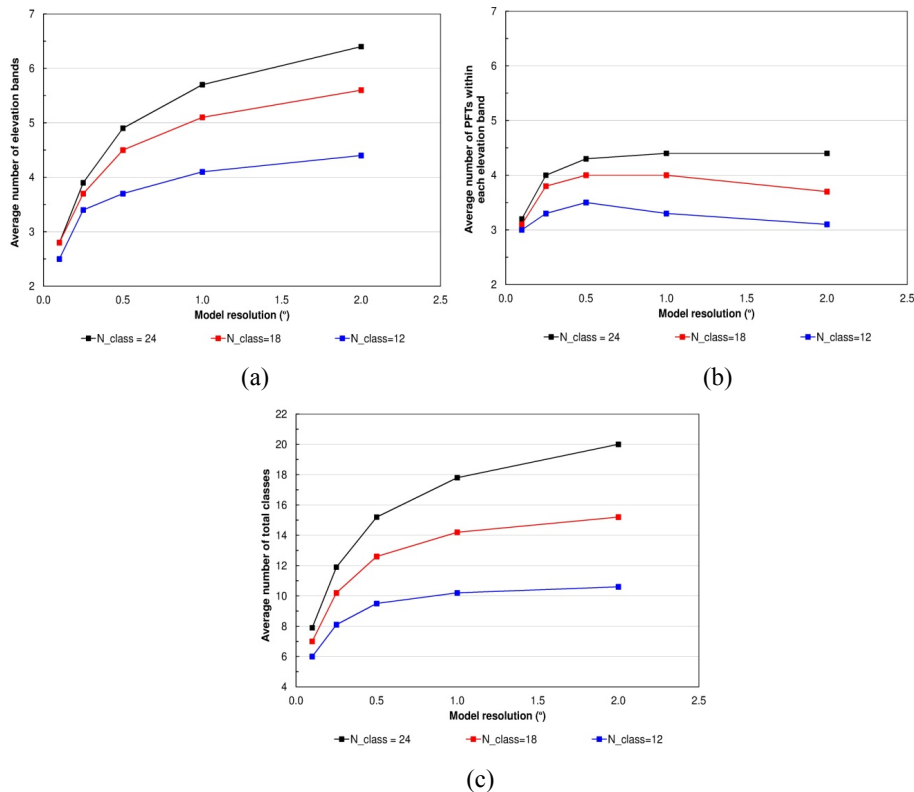


Fig. 7. SGC method with different maximum-allowed total classes N_{class} and at different resolutions. **(a)** Average number of elevation bands; **(b)** average number of PFTs within each elevation band; **(c)** average number of total classes. Black lines: $N_{\text{class}} = 24$; red lines: $N_{\text{class}} = 18$; blue lines: $N_{\text{class}} = 12$.

Enhancing the subgrid land surface representation in land surface models

Y. Ke et al.

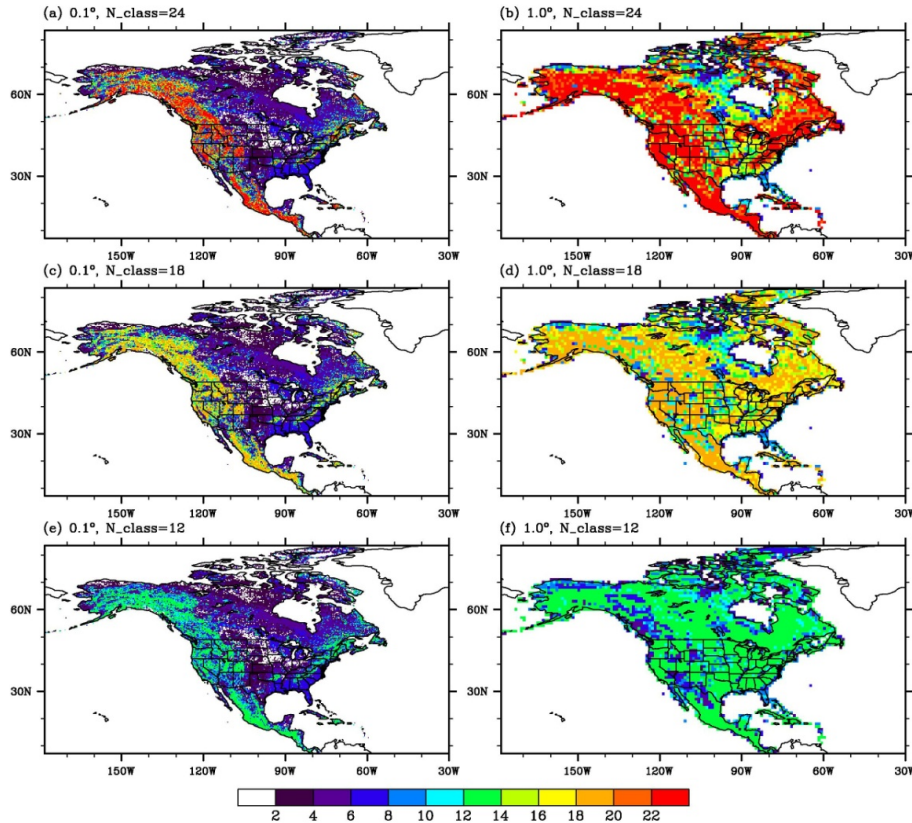


Fig. 8. Spatial distribution of number of total classes produced from the method for N_{class} of 24, 18 and 12 at 0.1° and 1.0° model resolution. **(a)** 0.1° , $N_{\text{class}} = 24$; **(b)** 1.0° , $N_{\text{class}} = 24$; **(c)** 0.1° , $N_{\text{class}} = 18$; **(d)** 1.0° , $N_{\text{class}} = 18$; **(e)** 0.1° , $N_{\text{class}} = 12$; **(f)** 1.0° , $N_{\text{class}} = 12$.

[Title Page](#)
[Abstract](#)
[Introduction](#)
[Conclusions](#)
[References](#)
[Tables](#)
[Figures](#)
[Back](#)
[Close](#)
[Full Screen / Esc](#)
[Printer-friendly Version](#)
[Interactive Discussion](#)

Enhancing the subgrid land surface representation in land surface models

Y. Ke et al.

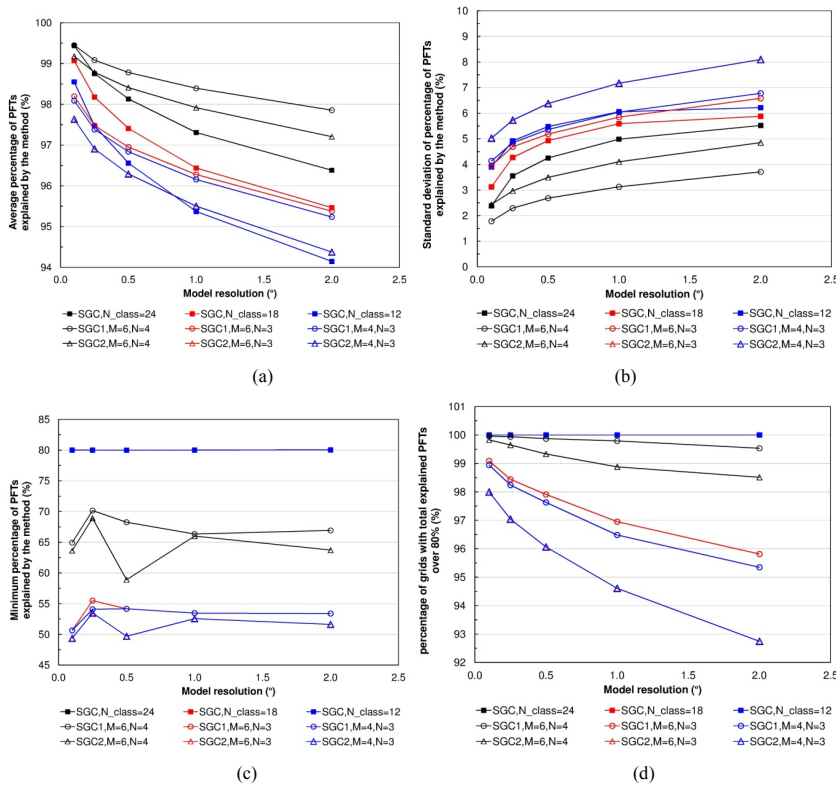


Fig. 9. Total PFTs explained by method SGC, SGC1 and SGC2 across NA. **(a)** Average percentage of PFTs explained within model grids; **(b)** standard deviation of PFT percentage explained within model grids; **(c)** minimum percentage of PFTs explained within model grids; **(d)** percentage of grids with total PFTs explained by the method over 80%. Black lines: $N_{class} = 24$; red lines: $N_{class} = 18$; blue lines: $N_{class} = 12$. Square symbol: SGC; circular symbol: SGC1; triangular symbol: SGC2.

[Title Page](#)

[Abstract](#)

[Introduction](#)

[Conclusions](#)

[References](#)

[Tables](#)

[Figures](#)

⏪

⏩

⏴

⏵

[Back](#)

[Close](#)

[Full Screen / Esc](#)

[Printer-friendly Version](#)

[Interactive Discussion](#)



Enhancing the subgrid land surface representation in land surface models

Y. Ke et al.

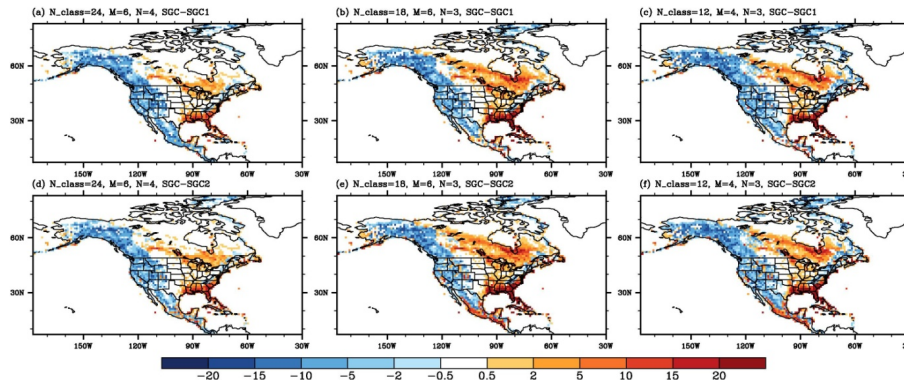


Fig. 10. Difference in percentage of total PFTs explained by SGC compared to SGC1 (top row), and SGC compared to SGC2 (bottom row) at 1.0° model resolution.

Title Page

Abstract

Introduction

Conclusions

References

Tables

Figures



Back

Close

Full Screen / Esc

Printer-friendly Version

Interactive Discussion

Enhancing the subgrid land surface representation in land surface models

Y. Ke et al.

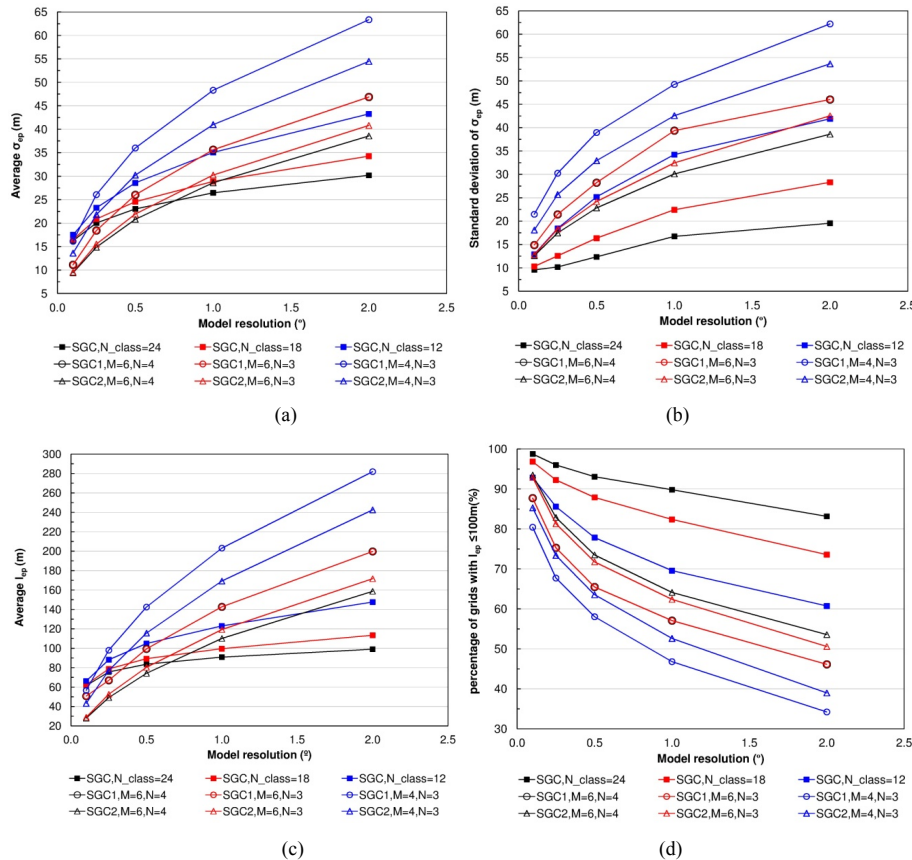


Fig. 11. Elevation variability explained by methods SGC, SGC1 and SGC2. **(a)** Average σ_{ep} ; **(b)** standard deviation of σ_{ep} ; **(c)** average l_{ep} ; **(d)** percentage of grids with $l_{ep} \leq 100$ m. Black lines: $N_{class} = 24$; red lines: $N_{class} = 18$; blue lines: $N_{class} = 12$. Square symbol: SGC; circular symbol: SGC1; triangular symbol: SGC2.

[Title Page](#)

[Abstract](#)

[Introduction](#)

[Conclusions](#)

[References](#)

[Tables](#)

[Figures](#)

[⏪](#)

[⏩](#)

[⏴](#)

[⏵](#)

[Back](#)

[Close](#)

[Full Screen / Esc](#)

[Printer-friendly Version](#)

[Interactive Discussion](#)

Enhancing the subgrid land surface representation in land surface models

Y. Ke et al.

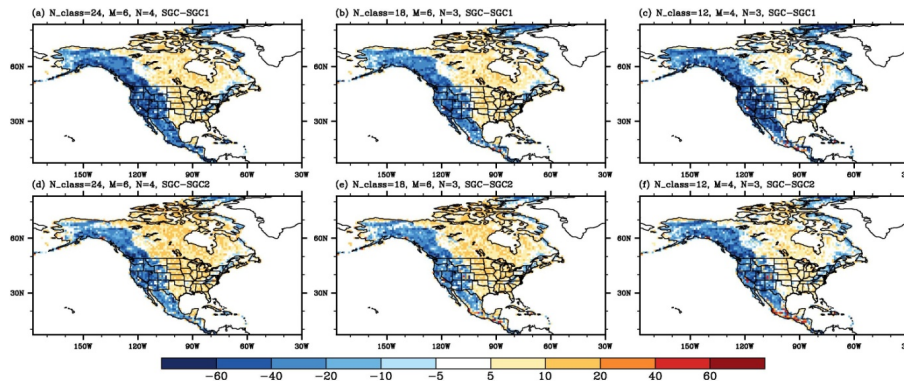


Fig. 12. Difference in average standard deviation of elevation for SGC compared to SGC1 (top row) and SGC compared to SGC2 (bottom row) at 1.0° model resolution.

Title Page

Abstract

Introduction

Conclusions

References

Tables

Figures



Back

Close

Full Screen / Esc

Printer-friendly Version

Interactive Discussion